Composites: Part A 180 (2024) 108083

Contents lists available at ScienceDirect

Composites Part A

journal homepage: www.elsevier.com/locate/compositesa

Magnetic guidance shape memory PLA/TBC/Fe_3O_4 microspheres for dentin tubule sealing

Tao Guo [a,1], Jiayuan Chen [b,1], Lan Luo [a], Qiangwang Geng [a], Linlin Wang [a], Fenghua Zhang [a,*], Narisu Hu [c,*], Yanju Liu [d], Jinsong Leng [a,*]

[a] Centre for Composite Materials and Structures, Harbin Institute of Technology (HIT), No. 2 Yikuang Street, Harbin 150080, PR China
[b] First Affiliated Hospital of Harbin Medical University, College of Stomatology, Harbin Medical University, No. 143 Yiman Street, Nangang District, Harbin 150001, PR China
[c] Oral Implant Center, Second Affiliated Hospital of Harbin Medical University, Harbin 150086, PR China
[d] Department of Astronautic Science and Mechanics, Harbin Institute of Technology (HIT), No. 92 West Dazhi Street, Harbin 150001, PR China

ARTICLE INFO

Keywords:
A. Smart materials
A. Biocomposite
B. Microstructures
D. Microstructural analysis

ABSTRACT

Shape memory polymer (SMP) microspheres possess controllable physicochemical properties, internal cavities capable of loading drugs or nanoparticles, and inherent intelligence, making them suitable for various biomedical applications. In this research, we utilized tri-n-butyl citrate (TBC) to lower the glass transition temperature of shape memory polylactic acid (PLA) to approximate oral temperature. Following this, we introduced oleic acid-modified Fe_3O_4 nanoparticles to confer magnetism to the material. Subsequently, SMP microspheres with a core–shell structure encapsulating Fe_3O_4 particles were prepared using the emulsion-solvent evaporation method, and we carefully controlled their particle size and morphology to match the diameter of dentinal tubules. Our investigation focused on applying these magnetically guided microspheres, which exhibited excellent shape memory performance, for sealing dentinal tubules. These microspheres displayed the ability to move directionally under the influence of a magnetic field. As a result, they could be attracted into the interior of dentinal tubules in their temporary shape and then revert to their initial shape upon heating at 40 °C, thereby achieving the closure of dentinal tubules effectively. The microsphere entry rate during the tubule closure process was found to be 93.33 ± 2.82 %, with a corresponding sealing rate of 85.41 ± 7.11 %. The successful demonstration of magnetic-guided movement and the utilization of the shape memory function for dentinal tubule sealing significantly expand the potential applications of SMP microspheres in the field of biomedical science.

1. Introduction

Shape memory polymers (SMPs) are a class of responsive polymeric materials that can temporarily retain a particular shape and then return to their original form when exposed to external stimuli like light, electricity, heat, or magnetism. SMPs possess several advantageous properties, including being lightweight, having the ability to undergo significant deformation, and featuring diverse driving mechanisms. These qualities make them intelligent materials capable of effectively integrating structural and functional aspects. As a result, SMPs have found extensive applications in various fields, such as aerospace, biomedical engineering, 4D printing, and soft robotics [1–8]. The growing demand for micro- and nanoscale materials in the biomedical domain has led to the evolution of intelligent deformable materials, including shape memory polymers, in the micro- and nanoscale range. This includes microspheres, microcapsules, and micro/nanofibers [9–11].

Polymer microspheres are polymeric particles with diameters ranging from micrometers to nanometers, and they possess a spherical morphology. Also known as organic microparticles or polymer microparticles, these microspheres offer diverse structures that grant unique properties, such as controllable physicochemical characteristics and internal cavities capable of encapsulating drugs or nanoparticles. Moreover, the molecular curling degree and orientation of polymer

* Corresponding authors.
E-mail addresses: fhzhang_hit@163.com (F. Zhang), hmuhunarisu@163.com (N. Hu), lengjs@hit.edu.cn (J. Leng).
[1] These authors contributed equally to this work.

https://doi.org/10.1016/j.compositesa.2024.108083
Received 12 October 2023; Received in revised form 27 January 2024; Accepted 7 February 2024
Available online 11 February 2024

microspheres can be altered, enabling controlled morphologies [12–14]. Due to these advantages, polymer microspheres have found widespread application in biomedical fields [15,16]. Various materials can be employed to fabricate polymer microspheres, with examples, including polylactic acid (PLA), poly(lactic-co-glycolic acid) (PLGA), polycaprolactone (PCL), polyurethane, and polyethylene glycol [17–21]. Among these materials, PLA microspheres have garnered significant attention from researchers due to their excellent biocompatibility and mechanical properties. For instance, Yuan et al. [22] produced PLA microspheres using the emulsion-ultrasonic atomization method and investigated the influence of ultrasonic atomization duration and PVA concentration on microsphere size and morphology. Additionally, Xu et al. [23] successfully fabricated injectable PLA microspheres with a high drug loading of bupivacaine using the oil-in-water emulsion solvent evaporation method. Furthermore, Zhan et al. [24] prepared PLA microspheres encapsulating Fe_3O_4 using the emulsion-solvent evaporation technique. Despite the extensive research on polymer microspheres, their applications have mainly focused on targeted drug delivery and drug release [25,26], with limited in-depth investigations and applications of shape memory microspheres. Consequently, research and development of shape memory microspheres hold significant importance in expanding the application areas of SMPs and polymer microspheres.

Shape memory microspheres are polymeric microspheres derived from SMPs, combining the advantageous features of both SMPs and polymeric microspheres, including exceptional shape memory performance and controllable physicochemical properties [27,28]. Zhang et al. [29] produced shape memory polyurethane microspheres with a core–shell structure using emulsion droplet interface polymerization and extensively studied their shape memory behavior. Guo et al. [30] developed light-responsive shape memory microspheres composed of poly(d,l-lactic acid) matrix encapsulating gold nanoparticles. Bai et al. [31] incorporated multi-walled carbon nanotubes (MWCNT) with high photothermal conversion efficiency into cellulose acetate (CA) microspheres using an improved emulsion-solvent evaporation method, resulting in CA microspheres capable of reverting to their initial shape under 808 nm near-infrared light irradiation. Shape memory polymers and their microsphere structures have significant potential in biomedicine [32–34], particularly in bone repair, tracheal stents, orbital implants, and other applications. However, the application of shape memory microspheres in dentistry remains limited at present.

Dentin hypersensitivity refers to toothache caused by external stimuli such as extreme cold or hot temperatures, acidic chemicals, and mechanical friction acting on the teeth. It is characterized by sudden, sharp pain that lasts for a short duration [35]. This symptom mainly results from tooth enamel wear or loss, leading to the exposure of dentin [36]. Currently, there are two primary approaches for treating dentin hypersensitivity. The first approach involves desensitizing the tooth nerves to inhibit their impulses, such as using desensitizing toothpaste containing fluoride [37] or applying other desensitizing agents like strontium chloride. The second approach for treating dentin hypersensitivity is to fill and seal the dentinal tubules [38] to prevent external stimuli from reaching the tooth nerves. Common sealing materials include gels [39], resins [40], and others. However, the first approach is challenging to maintain long-term effectiveness, as toothache symptoms may reoccur once the use of desensitizing agents is discontinued. The second approach has limitations concerning the depth of dentinal tubule sealing, as it typically only seals the surface layer. When the exposed dentin is subjected to mechanical stimulation again, the surface sealant is prone to dislodgement, leading to the reopening of dentinal tubules and resulting in secondary recurrence.

Based on the background provided, we opted for biocompatible shape memory polylactic acid (PLA) as the matrix for our study. To enhance the shape memory performance and reduce the transition temperature within the oral cavity's tolerable range, we incorporated tributyl citrate (TBC) into PLA. Additionally, we introduced oleic acid-modified magnetic Fe_3O_4 nanoparticles to impart a certain level of magnetism to the material, enabling controlled movement under an external magnetic field. Subsequently, we prepared the PLA/TBC material into shape memory microspheres using the emulsion-solvent evaporation method, ensuring precise control over the morphology and particle size of the microspheres. During this preparation process, we introduced oleic acid-modified Fe_3O_4 particles, resulting in PLA/TBC/Fe_3O_4 microspheres with magnetic-directed movement capabilities, the ability to recover their initial shape slightly above oral temperature (40 °C), excellent biocompatibility, and matching the diameter of dentinal tubules. Furthermore, we investigated the feasibility of utilizing these microspheres for dentinal tubule sealing and evaluated their sealing efficacy.

2. Experimental sections

2.1. Materials

Polylactic acid (PLA) was procured from Natureworks LLC (USA) under the product model PLA 4032D. Tributyl citrate (TBC, >98 %) was obtained from Shanghai Aladdin Bio-Chem Technology Co., Ltd. (China). We used analytical-grade dichloromethane (DCM) from Tianjin Fuyu Fine Chemical Co., Ltd. (China) for the experiments. Nanoscale Fe_3O_4 (10 nm) modified with oleic acid was purchased from Zhongke Leiming Technology Co., Ltd. (China). Additionally, we acquired two types of polyvinyl alcohol (PVA) with distinct molecular weights: one was alcohol-soluble with a molecular weight of 14,500 from Shanghai Aladdin Bio-Chem Technology Co., Ltd. (China), and the other, water-soluble with a molecular weight range of 8,500–12,400 from Sigma-Aldrich Co. LLC (USA).

2.2. Preparation of shape memory PLA/TBC/Fe_3O_4 composites

The PLA raw material underwent a drying process in an oven at 50 °C for 6 h to remove surface moisture. Subsequently, we weighed 5 g of PLA/TBC in different proportions to prepare PLA/TBC mixtures with mass ratios of 100/0, 94/6, 91/9, 88/12, 85/15, and 82/18. Each blend was mixed with a specific mass of dichloromethane and stirred at 300 r/min for 6 h to ensure complete dissolution of PLA and uniform mixing with TBC, resulting in PLA/TBC solutions with a concentration of 18 wt %. These solutions were poured into square molds measuring 8 cm * 8 cm and placed in a fume hood for 24 h to allow the solvent to evaporate. After reaching a constant weight due to drying, the samples in the molds were de-molded to obtain different proportions of PLA/TBC materials. We conducted differential scanning calorimetry (DSC), thermogravimetric analysis (TGA), and shape memory performance testing on the different PLA/TBC materials to determine the optimal ratio of PLA/TBC. Based on the optimal ratio, oil-modified nano-sized Fe_3O_4 particles in the range of 5 to 15 wt% were introduced into the dichloromethane solution (18 wt% PLA/TBC). The mixture was then subjected to ultrasonic treatment for 30 min to ensure the uniform dispersion of Fe_3O_4 particles in the solution. Finally, we obtained the prepared PLA/TBC/Fe_3O_4 composite materials through a 24 h evaporation process followed by demolding.

2.3. Preparation of shape memory PLA/TBC/Fe_3O_4 microspheres

To prepare the PLA85/TBC15 composite material, it was dissolved in dichloromethane to create an oil phase solution with a specific concentration. Simultaneously, the alcohol-soluble PVA was heated (100 °C) and stirred until it dissolved in deionized water, forming a water phase solution with a specific concentration. Subsequently, a 20 mL oil phase solution was combined with a 20 mL water phase solution, and a disperser (T25 digital ULTRA-TURRAX, IKA, Germany) was used at a designated speed to stir the mixture for 1 h, ensuring thorough emulsification. Once emulsification was complete, an additional 40 mL

of deionized water was added to the solution while continuing the stirring for 1 h to evaporate the organic solvent present. To remove any remaining dichloromethane, the solution was placed on a heating plate at 60 °C, leading to the formation of a microsphere suspension. The obtained microsphere suspension was allowed to settle, the supernatant was discarded, and deionized water was added for washing. This washing process was repeated three times to obtain PLA/TBC microspheres.

During the microsphere preparation process, we applied the controlled variable method to vary the concentration of the polymer in the oil phase (10 mg/mL, 30 mg/mL, 50 mg/mL), the concentration of the emulsifier in the water phase (0.5 wt%, 1 wt%, 2 wt%), and the stirring speed of the disperser (3000 rpm, 5000 rpm, 7000 rpm) to produce microspheres with a particle size matching the diameter of dentinal tubules. This allowed us to determine the optimal parameters for microsphere preparation. Based on these optimal parameters, oleic acid-modified nanoscale Fe_3O_4 particles were introduced into the oil phase solution at a mass percentage of 15 wt% compared to the solute. By repeating the aforementioned steps, we successfully obtained PLA/TBC/Fe_3O_4 microspheres.

2.4. Differential scanning calorimetry

The DSC instrument used in this research was the DSC1 differential scanning calorimeter from Mettler-Toledo, Switzerland. For the testing of samples, the following parameters were employed: the ambient atmosphere consisted of nitrogen gas, the temperature range was set from 20 to 190 °C, the heating rate was 10 °C/min, and the temperature accuracy was ± 0.2 °C. During the testing process, the sample underwent an initial heating cycle to eliminate its thermal history. The data obtained during the second heating cycle were then analyzed to determine essential parameters of the sample, such as the glass transition temperature (T_g), crystallization temperature (T_c), melting temperature (T_m), and other related characteristics.

2.5. Thermogravimetric analysis

In this study, the TGA equipment employed was the TGA1 thermogravimetric analyzer, purchased from Mettler-Toledo, a Switzerland-based company. The testing parameters for the samples included a nitrogen gas environmental atmosphere, a testing temperature range from 30 to 500 °C, and a heating rate of 10 °C/min.

2.6. Micro analysis

The morphology and structure of the microspheres, Pt-sputtered for 30 s, were characterized using a scanning electron microscope (SEM, SU500, Hitachi, Japan). The particle size distribution of the microspheres under different preparation conditions was determined using Image J software. To observe the encapsulation and distribution of Fe_3O_4 particles in the microspheres, a transmission electron microscope (TEM, Talos F200X G2, Thermo Fisher Scientific, Czech) was used. Further analysis of the distribution of Fe_3O_4 particles within the microspheres was performed using energy-dispersive X-ray spectroscopy (EDS). Cone-shaped variable magnetic field analysis was conducted on the microspheres to analyze magnetic-directed movement. An electromagnetic coil system was self-assembled for magnetic field control, with adjustments made to the coil system parameters to control the magnetic field's intensity. The magnetic core on the coil was controlled by signals generated from relevant software in the computer. To ensure proper functioning, circulating water was used to cool the interior of the coil. A 10 μL microsphere solution was pipetted onto a glass slide, which was then placed in the center of the magnetic coil on an inverted microscope stage. The magnetic field type was set to a cone-shaped variable magnetic field with a frequency of 10 Hz and an amplitude of 1 V. The movement of the microspheres was observed and recorded using an inverted optical microscope.

2.7. Shape memory behavior

The sample was shaped into a long strip (40 mm × 8 mm × 1 mm) and then heated above the glass transition temperature to form a temporary "U-shape." The load was released after cooling to room temperature, resulting in a temporary "U-shaped" strip. After 8 h at room temperature, the change in the material's angle was recorded. Subsequently, the strip was heated again above the glass transition temperature, and the shape recovery behavior at various time intervals was recorded using a camera. The shape fixity ratio (R_f) and shape recovery ratio (R_r) of the sample were calculated using Equations (1) and (2), respectively. In these equations, θ_α represents the angle at which the long strip sample was bent into the "U-shape," θ_β represents the difference in bending angle before and after shape fixation, and θ_γ represents the difference in bending angle before and after shape recovery of the long strip sample.

$$R_f = \frac{\theta_\alpha - \theta_\beta}{\theta_\alpha} \times 100\% \quad (1)$$

$$R_r = \frac{\theta_\alpha - \theta_\gamma}{\theta_\alpha} \times 100\% \quad (2)$$

2.8. Biocompatibility

We first carried out cytotoxicity experiments in vitro. To assess the effect of different concentrations of PLA/TBC/Fe_3O_4 microspheres on the cell viability of human gingival fibroblasts (HGFs) cells, a CCK-8 assay was performed. The following steps were undertaken: the PLA/TBC/Fe_3O_4 microsphere solution was exposed to ultraviolet light for 30 min to ensure sterilization. The microspheres were added to a 96-well plate with a cell density of 1×10^4 cells/well, HGF cells were treated with various concentrations of microspheres (0 μg/mL, 62.5 μg/mL, 125 μg/mL, 250 μg/mL, and 500 μg/mL) in a 96-well plate. The cells were then cultured at 37 °C in a 5 % CO_2 environment for 24 h. After that, 200 μL of the microsphere solution at different concentrations was added to each well, followed by another 24-hour incubation at 37 °C in a 5 % CO_2 environment. Subsequently, 10 μL of CCK-8 solution was added to each well and incubated for 3 h. The absorbance of each group was measured at a wavelength of 450 nm using an enzyme-linked immunosorbent assay (ELISA) reader. The relative cell viability was calculated using Equation (3), where A_s represents the absorbance of the experimental wells, A_c represents the absorbance of the control group, and A_b represents the absorbance of the blank wells.

$$CellViability(\%) = \frac{A_s - A_b}{A_c - A_b} \times 100\% \quad (3)$$

To assess the safety of the microspheres in vivo, we conducted a study using 16 female Balb/c mice. Before the experiment, the mice were allowed to acclimate for 7 days. Subsequently, they were randomly divided into two groups, with 8 mice in each group. Group A served as the control group and received treatment with physiological saline, while Group B served as the treatment group and received treatment with 1 mg/mL of PLA/TBC/Fe_3O_4 microspheres. The respective treatments were administered for 14 days. After the treatment period, the mice were euthanized, and histological examinations were performed on the heart, liver, spleen, lungs, and kidneys using H&E staining. This analysis aimed to evaluate the in vivo safety of the PLA/TBC/Fe_3O_4 microspheres.

2.9. Dentin tubule sealing test

The ex vivo tooth samples used in this research were extracted from third molars and premolars at the Department of Oral Surgery, the

Second Affiliated Hospital of Harbin Medical University. Before sample collection, informed consent was obtained from the patients, ensuring ethical compliance. Only intact teeth without damage, caries, or hidden cracks were selected to ensure sample quality. The tooth samples underwent manual removal of soft tissues and dental calculus on the root surface using a scaler. Subsequently, they were ultrasonically cleaned in deionized water for 5 min and stored in physiological saline at 4 °C until further use. Diamond discs were used for low-speed cutting with water cooling to process the tooth samples. The tooth crowns were vertically sectioned along the long axis of the tooth at the enamel-dentin junction, removing the enamel part. This process yielded dentin discs of approximately 1 mm thickness, with the experimental surface facing the crown of the tooth. The experimental surface was then manually polished using 240, 600, and 1200-grit silicon carbide papers. Next, the dentin discs were subjected to acid-etching in a 10 % ethylenediaminetetraacetic acid disodium salt (EDTA) solution for 2 min, followed by ultrasonic cleaning for 10 min, and then stored in physiological saline at 4 °C. The thirty prepared dentin discs were randomly divided into three groups, with ten discs in each group. Group A served as the blank control group, Group B as the experimental group, and Group C as the positive control group.

Each group of samples was processed as follows:

Group A: The dentin discs were immersed in deionized water for 5 min with the application of an external magnetic field.

Group B: The dentin discs were immersed in a 500 μg/mL solution of stretched 100 % microspheres for 5 min with the application of an external magnetic field.

Group C: The dentin discs were immersed in a 500 μg/mL solution of stretched 100 % microspheres for 5 min without the application of an external magnetic field.

To evaluate the effectiveness of microsphere sealing of dentinal tubules under different conditions (presence or absence of a magnetic field), we conducted statistical analysis on scanning electron microscope (SEM) images of microsphere-sealed dentin tubules. The entry efficiency (D_e) and sealing efficiency (D_s) of the microspheres into the dentinal tubules were calculated using Equations (4) and (5), respectively. In

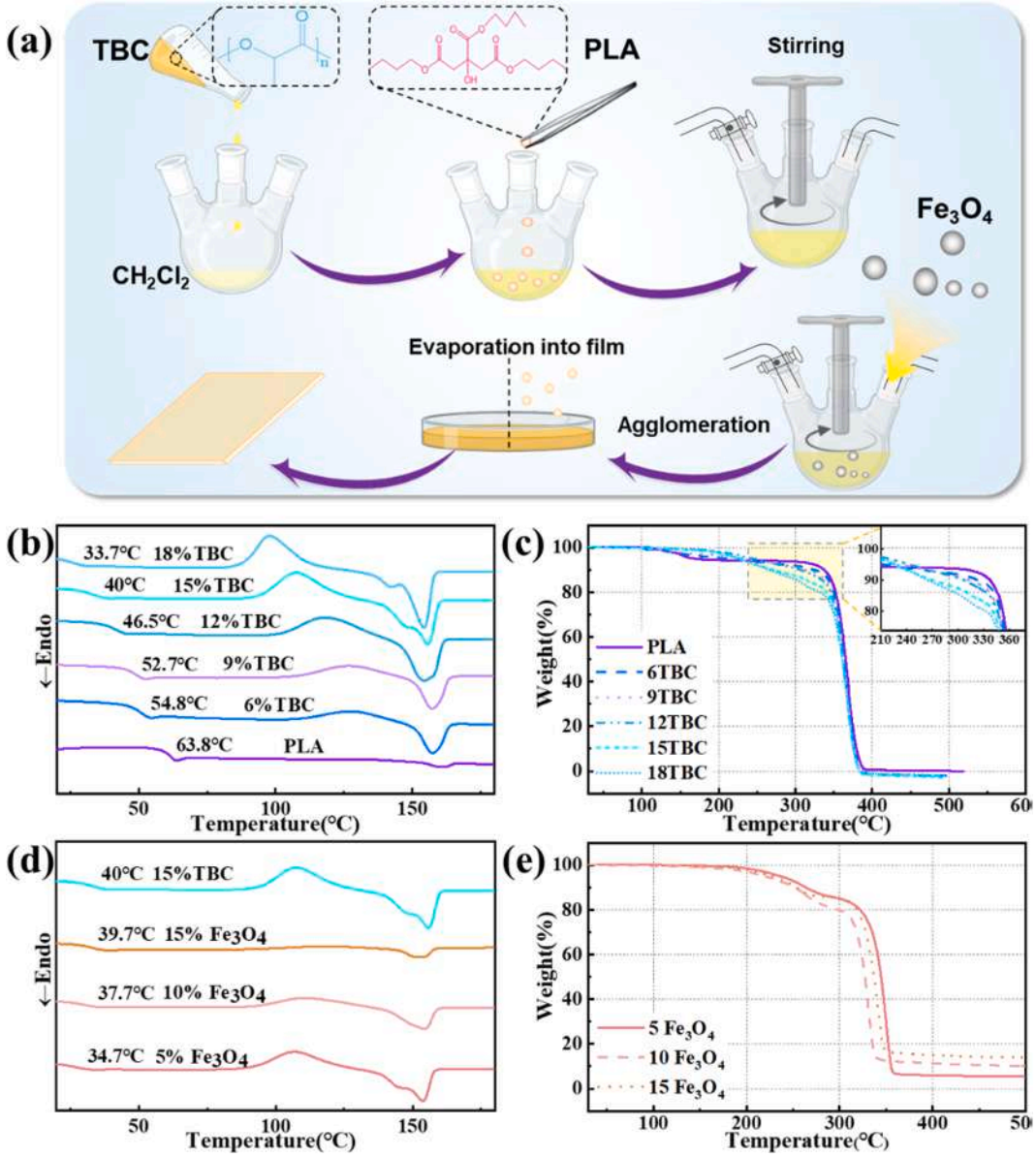

Fig. 1. (a) Flow chart for the preparation of PLA/TBC/Fe_3O_4 materials; (b) DSC curves of different ratios of PLA/TBC materials; (c) TGA curves of different ratios of PLA/TBC materials; (d) DSC curves of different ratios of Fe_3O_4 added to PLA85/TBC15 material; (e) TGA curves of different ratios of Fe_3O_4 added to PLA85/TBC15 material.

these equations, θ_t represents the total number of dentinal tubules, θ_s represents the number of dentinal tubules sealed by microspheres, and θ_e represents the number of microspheres that entered the dentinal tubules. Successful penetration was defined as the presence of at least one microsphere within a dentinal tubule. In contrast, successful sealing was defined as microspheres sealing more than 50 % of the surface area of each dentinal tubule.

$$D_e = \frac{\theta_e}{\theta_t} \times 100\% \quad (4)$$

$$D_s = \frac{\theta_s}{\theta_t} \times 100\% \quad (5)$$

Following the calculation of entry efficiency (D_e) and sealing efficiency (D_s) of the microspheres, the experimental data were subjected to statistical analysis using SPSS 25.0 statistical analysis software. Experimental data that exhibited a normal distribution were presented as mean standard deviation. The sealing and penetration rates between groups were compared using an independent samples *t*-test. Statistical significance was considered when $P < 0.05$. Subsequently, the obtained data were visually presented in the form of a bar chart for better illustration.

3. Results and discussion

3.1. Preparation and characterization of composite materials

Fig. 1(a) shows the flowchart for the preparation of PLA/TBC/Fe_3O_4 material. Fig. 1(b) illustrates the DSC curve of PLA, displaying its glass transition temperature, corresponding to its shape memory temperature of approximately 65 °C. This temperature is significantly higher than the typical temperature in the human oral cavity (36.5–37.2 °C). To make it suitable for oral applications, we incorporated TBC, which effectively lowers the shape memory temperature. The DSC data reveals that with increasing TBC content, the shape memory temperature of the material decreases. At a TBC content of 15 wt%, the shape memory temperature reduces to 40 °C. Furthermore, Fig. 1(c) shows that the addition of TBC influences the material's thermal stability, but it does not compromise its applicability in the oral environment.

In dentistry, the structure of dentinal tubules resembles a honeycomb porous structure. To facilitate the entry of shape memory microspheres into the dentinal tubules, these microspheres need to exhibit directional

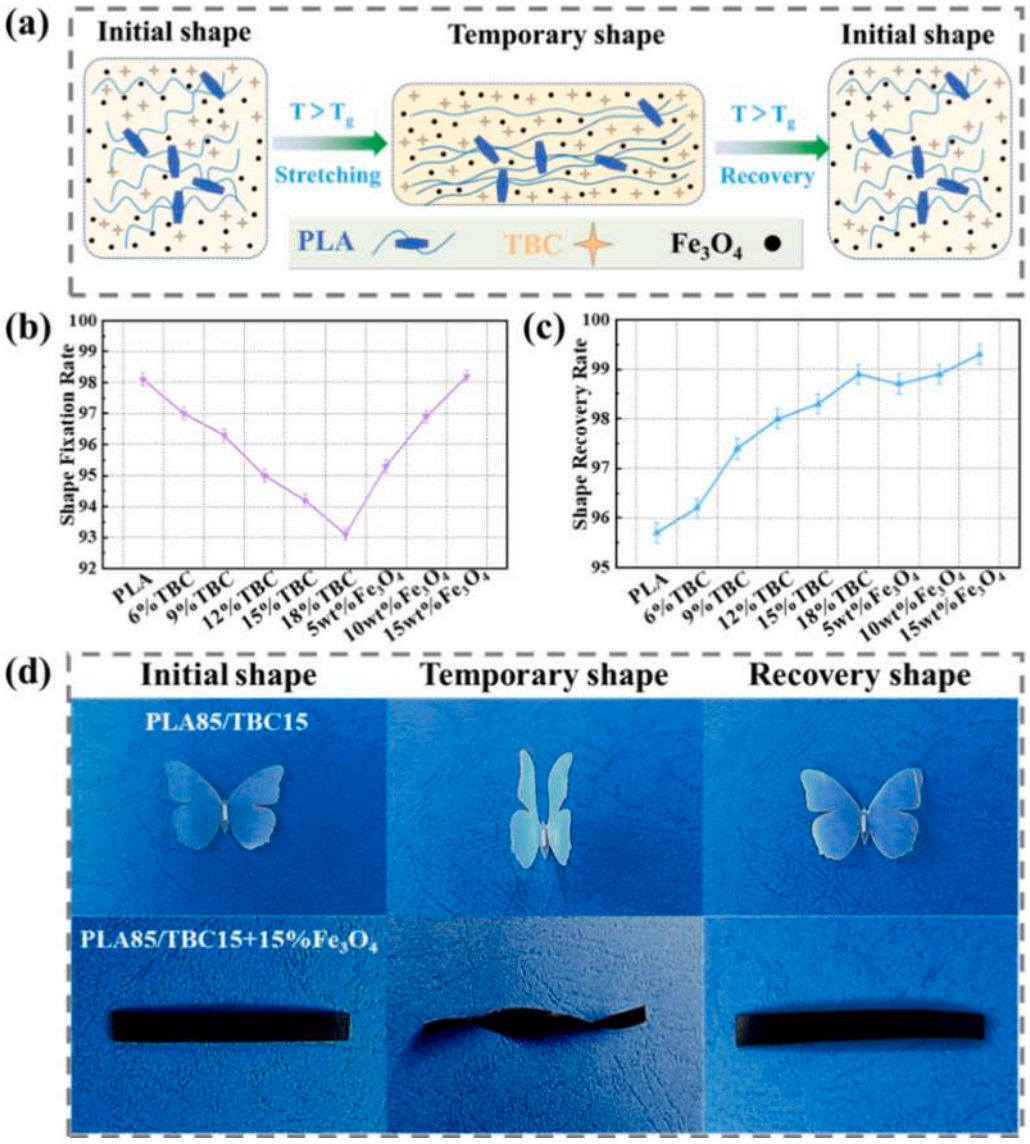

Fig. 2. (a) Shape memory mechanism diagram of PLA/TBC/Fe_3O_4 materials; (b) Line graph of shape fixation rate for different materials; (c) Line graph of shape fixation rate for different materials; (d) Shape Memory Performance Testing of Different Materials.)

movement under external intervention. However, PLA/TBC materials lack this capability of directional movement under external stimuli. To address this, we incorporated nano-sized Fe_3O_4 particles, a commonly used magnetic material, into PLA/TBC, resulting in PLA/TBC/Fe_3O_4 composite materials with magnetic orientation functionality. Fig. 1(d) and 1(e) demonstrate that the addition of Fe_3O_4 particles influences the T_g and thermal stability of the material. At a Fe_3O_4 particle content of 15 wt%, the shape memory temperature of the material is comparable to that of PLA85/TBC15, with a value of 39.7 °C. Although this temperature is slightly higher than the oral cavity's temperature, it falls within the acceptable range for oral applications and remains within the optimal working temperature range for shape memory microspheres. Additionally, while the addition of Fe_3O_4 particles affects the material's thermal stability, it does not compromise its suitability for oral applications.

3.2. Shape memory properties of composite materials.

Moreover, we conducted experiments to assess the shape memory properties of composite materials, namely PLA, PLA85/TBC15, and PLA85/TBC15 + 15 wt% Fe_3O_4. Fig. 2 (a) depicts the mechanism of shape memory in PLA/TBC/Fe_3O_4 material. The molecular chain segments of the PLA/TBC/Fe_3O_4 material consist of a rigid segment in the form of a crystalline region and a flexible segment in the amorphous state. When the external temperature is higher than the material's T_g, both the rigid and flexible segments of the molecular chains exhibit enhanced mobility. Under the influence of external loads, the material can undergo deformation, and the molecules in the rigid and flexible segments can freely move. Subsequently, as the temperature decreases below T_g, the rigid segments reorganize to form a crystalline region, while the flexible segments solidify in their original shape. Macroscopically, this results in the material retaining a temporary shape. Upon reheating above T_g, the mobility of the molecules in both the rigid and flexible segments is restored, leading to the material reverting to its initial shape. The R_f and R_r of these materials were determined and depicted in Fig. 2(b) and Fig. 2(c), respectively. The figures reveal that the incorporation of TBC led to a gradual decrease in R_f while increasing R_r. For instance, PLA exhibited a swift recovery to its original shape within 54 s at 65 °C, with R_f and Rr at 98.1 % and 95.7 %, respectively. Upon adding 15 wt% TBC, the composite material could restore the temporary "U" shape to its initial form within 25 s under a 40 °C heat source, but with a decrease in R_f to 94.2 % and an increase in R_r to 98.3 %.

Additionally, the introduction of Fe_3O_4 had a positive impact on the shape memory performance. At 15 wt% Fe_3O_4 content, the material displayed a rapid recovery to its initial shape within 23 s when exposed to a 40 °C heat source, with R_f and Rr values of 98.2 % and 99.3 %, respectively. Fig. 2(d) depicts the process of cutting PLA85/TBC15, and PLA85/TBC15 + 15 wt% Fe_3O_4 materials into various shapes to validate their shape memory functionality. Based on the data presented above, the PLA85/TBC15 + 15 wt% Fe_3O_4 composite material exhibited exceptional shape memory performance, making it well-suited for applications within the human oral cavity.

The effect of the addition of TBC and Fe_3O_4 on the T_g, R_f, and R_r of the material can be explained by the following two aspects: TBC has good compatibility with PLA, and the interaction between the two reduces the force between the PLA macromolecules, which makes the movement of the chain segments easier. In addition, the addition of TBC also provides more "free space" for the movement of PLA's chain segments, which makes the movement of chain segments and the rearrangement of chain segments easier, so the T_g and R_f of the material will be significantly reduced with the increase of TBC content, but the R_r of the material increases with increasing TBC content. However, Fe_3O_4 and PLA are mutually incompatible two phases, and the addition of Fe_3O_4 will form a spatial site resistance in the polymer matrix, thus increasing the force between PLA macromolecules, making the movement of the chain segments more difficult, thus hindering the crystallization process of the matrix material and destroying the integrity of the crystallization of the material to a certain extent. Therefore the T_g and R_r of the material show a decreasing trend when a small amount of Fe_3O_4 particles are added to the material. However, as a reinforcing phase, the elevated content of Fe_3O_4 particles will play a certain reinforcing effect on the matrix material, so the T_g and R_r of the material will rise again with the increase of the content of Fe_3O_4 particles.

3.3. Preparation and characterization of microspheres

The emulsion-solvent evaporation method is a widely used, simple, and highly controllable manufacturing technique for preparing polymer microspheres. Preliminary experiments have demonstrated that the emulsion-solvent evaporation method can be employed to produce shape-memory polymer microspheres from the PLA85/TBC15 material system. Fig. 3(a) (I) displays the SEM image of the PLA/TBC microspheres prepared using this method. SEM was also utilized to examine broken microspheres to ascertain the microsphere structure, as depicted in Fig. 3(a) (II, III). The SEM images of the damaged microspheres reveal the presence of internal voids, suggesting that the prepared PLA/TBC microspheres possess a hollow core–shell structure. To further validate the structure of the polymer microspheres, transmission electron microscopy (TEM) was employed, and Fig. 3(a) (IV) presents the TEM image of the PLA/TBC microspheres, confirming the presence of a core–shell structure.

The diameter of dentinal tubules in tooth dentin typically ranges from 3 to 4 μm. To prepare shape memory microspheres capable of completely occluding dentinal tubules, the microsphere size needs to be slightly larger than the diameter of the dentinal tubules. This ensures a perfect fit of the microspheres into the dentinal tubules, effectively sealing them.

Firstly, the impact of polymer concentration on the morphology, size, and size distribution of microspheres based on the PLA85/TBC15 material system was investigated. The aqueous phase contained 1 wt% PVA, and the stirring speed was set at 7000 rpm. The polymer concentrations in the oil phase were 10 mg/mL, 30 mg/mL, and 50 mg/mL, respectively. Fig. 3(b) presents the SEM images and size distribution of the microspheres. As the PLA/TBC concentration in the oil phase increased, the average diameter of the microspheres gradually increased, and the diameter distribution became more dispersed, leading to a broader range of diameter gradients and a transformation of the microsphere surface from smooth to wrinkled.

At a PLA/TBC concentration of 10 mg/mL, the microsphere surface appeared smooth, with a diameter distribution ranging from 0.7 μm to 4.8 μm, and an average diameter of 3.16 μm. Higher PLA/TBC concentrations in the oil phase hindered the volatilization of the organic solvent. Consequently, after preparation, some residual organic solvents remained inside the microsphere cavities. During storage, the organic solvent evaporated at different rates in different parts of the microspheres, resulting in the appearance of wrinkles and depressions on the microsphere surface. Moreover, with the increase in PLA/TBC concentration in the oil phase, the number of oil phase droplets after stirring also increased. This, in turn, raised the probability of collisions among oil-phase droplets in the aqueous phase, leading them to fuse back together and form larger droplets. Consequently, this process resulted in increased microsphere size and broader size distribution.

Furthermore, the impact of emulsifier concentration in the aqueous phase on the morphology, size, and size distribution of microspheres was investigated. The PLA/TBC concentration in the oil phase was set at 10 mg/mL, and the mixer operated at 7000 rpm. The emulsifier concentrations in the aqueous phase were 0.5 wt%, 1 wt%, and 2 wt%, respectively. Fig. 3(c) presents the SEM images and size distribution of the microspheres. In this concentration range, the variation in emulsifier concentration had minimal impact on the surface morphology of the microspheres. However, an increase in PVA concentration in the

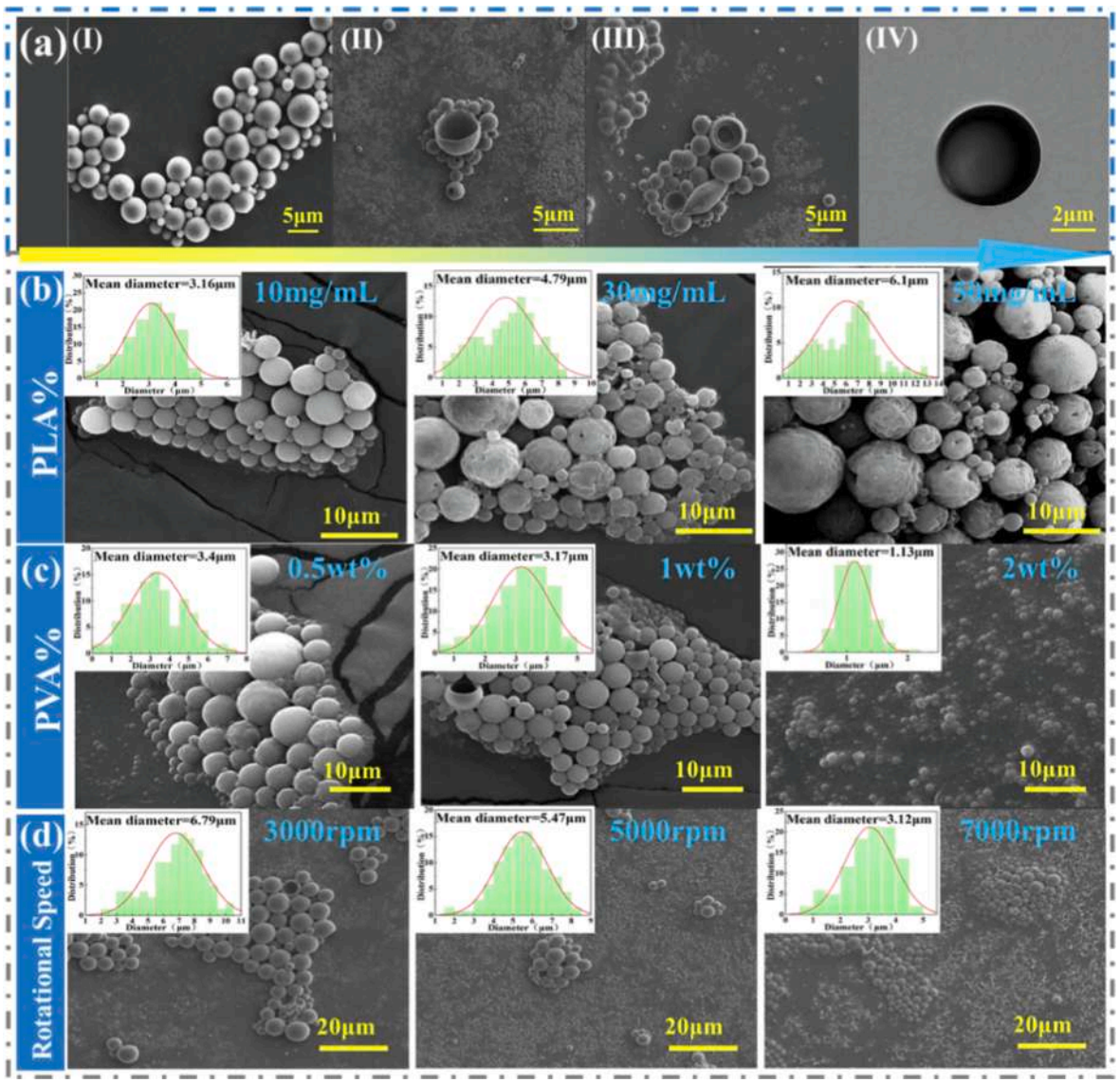

Fig. 3. (a) (I) SEM image of PLA/TBC microspheres (II) (III) SEM image of broken PLA/TBC microspheres (IV) TEM image of PLA/TBC microspheres; (b) SEM and diameter distribution of microspheres prepared with polymer concentrations of 10 ~ 50 mg/mL; (c) SEM and diameter distribution of microspheres prepared with emulsifier concentrations of 0.5 ~ 2 wt%; (d) SEM and diameter distribution of microspheres prepared with stirring speed of 3000 ~ 7000 rpm.

aqueous phase led to a gradual reduction in the average diameter of the PLA/TBC microspheres, resulting in a narrower range of diameter gradients. At a PVA concentration of 1 wt%, the average diameter of the prepared microspheres ranged from 0.6 μm to 4.8 μm, with an average diameter of 3.17 μm. A higher PVA concentration reduced the interfacial tension between the aqueous and oil phases, creating increased spatial hindrance among the oil phase droplets during stirring, thereby enhancing stability during the mixing process. Moreover, an elevated PVA concentration in the aqueous phase facilitated the formation of a protective interface film on the droplets' surface, preventing them from merging into larger entities upon collision. Consequently, an increasing PVA concentration resulted in smaller microspheres with a more uniform size distribution.

Subsequently, the impact of stirring speed on the morphology, size, and size distribution of the microspheres was investigated. The PLA/TBC concentration in the oil phase was 10 mg/mL, and the aqueous phase contained 1 wt% emulsifier. Stirring speeds of 3000 rpm, 5000 rpm, and 7000 rpm were applied. SEM images and size distribution in Fig. 3(d) illustrate the prepared microspheres. Within this concentration range, the stirring speed had minimal effect on the surface morphology of the microspheres. However, as the stirring speed increased, the average diameter of PLA/TBC microspheres gradually decreased, leading to a narrower range of diameter gradients. At 7000 rpm, the diameter of the microspheres ranged from 0.8 μm to 4.56 μm, with an average of 3.12 μm. Higher stirring speeds increased shear stress, which, in turn, redispersed secondary aggregates of small droplets during stirring, leading to a stable solution system and reduced microsphere size. Moreover, elevated stirring rates decreased the droplet size of the oil phase due to increased shear stress, resulting in faster evaporation of the organic solvent from small droplets, leading to a more uniform size distribution of the microspheres.

After investigating the effects of the three preparation parameters on microsphere morphology, size, and size distribution, it was found that microspheres prepared with a polymer concentration of 10 mg/mL, emulsifier concentration of 1 wt%, and stirring speed of 7000 rpm exhibited the most uniform size distribution, with the majority ranging from 3 to 4 μm. These microspheres are ideal for occluding dentinal tubules.

3.4. Motion of microspheres under the action of an applied magnetic field

To enable the microspheres to autonomously enter dentinal tubules, directed motion under external stimuli is crucial. Therefore, after determining the preparation parameters, we introduced oil-modified nano-sized Fe_3O_4 particles into the oil phase solution during the microsphere preparation process, resulting in the formation of PLA/TBC/Fe_3O_4 microspheres. Fig. 4(a) illustrates the production of PLA/TBC/Fe_3O_4 microspheres using the emulsion-solvent evaporation method. Fig. 4(b) and 4(c) display the SEM, TEM, and EDS images of the microspheres. It can be observed that the addition of magnetic particles did not significantly affect the microsphere size and morphology. The microspheres exhibited a high coverage of magnetic particles, and the magnetic particles were uniformly dispersed within the shell layer of the polymer microspheres. This high coverage and uniform dispersion of magnetic particles are advantageous for the microspheres' directed motion under the influence of a magnetic field.

Fig. S1 shows the complete trajectory of PLA/TBC/Fe_3O_4 microspheres in a triangular magnetic field. Fig. 4(d) and movie(S1-S6) illustrates the motion trajectory of PLA/TBC/Fe_3O_4 microspheres in different shapes of magnetic field. The microspheres exhibit directed motion under the influence of the applied magnetic field, aligning their motion direction with the direction of the magnetic field. To assess whether the motion direction of PLA/TBC/Fe_3O_4 microspheres can change with the magnetic field's direction, we observed the motion of other microspheres within the field of view after adjusting the magnetic field's orientation. When the direction of the magnetic field changes, the motion direction of PLA/TBC/Fe_3O_4 microspheres also adjusts accordingly, aligning with the new direction of the magnetic field. In addition, we applied a circulating magnetic field to examine the continuity of the microspheres' motion in the magnetic field, and the results showed that the microspheres could move continuously with the circulation of the magnetic field. These experimental observations suggest that PLA/TBC/Fe_3O_4 microspheres have the capability to enter dentinal tubules under the influence of a magnetic field, indicating their potential for targeted delivery within the dentinal tubules.

3.5. Shape memory properties of microspheres

Fig. 5(a) illustrates the process of programming the microspheres into temporary shapes and achieving shape memory. Initially, spherical microspheres are transformed into temporary ellipsoidal shapes. The prepared PLA/TBC/Fe_3O_4 microspheres are mixed with water-soluble PVA of a specific concentration. The mixture is then poured into an 8 cm × 8 cm mold and allowed to evaporate at room temperature for 24 h naturally. After complete evaporation, the PVA film embedded with microspheres is demolded, cut into 1 cm × 8 cm strips, softened by heating (100 °C), and stretched to 150 %, 200 %, and 250 % of its original length, respectively. During this stretching process of the polymer film, the microspheres' shape gradually transforms from spherical to ellipsoidal. Once cooled to room temperature, the microspheres maintain their temporary ellipsoidal shape. Subsequently, by dissolving the stretched PVA film in water, microspheres with varying degrees of stretching (PLA/TBC/Fe_3O_4) are obtained. Samples of microspheres stretched to different extents are then taken for SEM imaging to observe their temporary shapes. Following this, a small amount of microsphere solution is heated at 40 °C for 2 min on a heating platform to uniformly heat the microspheres. After heating, samples are taken and observed to verify the functionality of the microspheres' shape memory.

In Fig. 5(b), SEM images of the microspheres illustrate their initial shape, temporary shape, and shape after heating. The deformation of the microspheres increases with the degree of stretching of the PVA film. As the stretching degree of the PVA film rises, the transition of the microspheres from a spherical to an elliptical shape becomes more pronounced. Moreover, the PLA/TBC/Fe_3O_4 microspheres can withstand stretching up to a relative elongation of 150 % to 250 % without experiencing rupture. Furthermore, microspheres stretched to different ratios exhibit shape memory performance after the heating process, reverting from the elliptical shape back to the spherical shape, with a good shape recovery rate. These observations indicate that the PLA/TBC/Fe_3O_4 microspheres possess shape memory capabilities, enabling them to effectively seal the dentinal tubules.

3.6. Biocompatibility of microspheres

To assess the biological applicability of microspheres, we conducted CCK-8 experiments using PLA/TBC/Fe_3O_4 microsphere solutions at different concentrations. The results of the CCK-8 experiment are depicted in the column chart in Fig. S2. When the concentration range of PLA/TBC/Fe_3O_4 microspheres was within 500 μg/mL, the different concentrations of PLA/TBC/Fe_3O_4 microsphere solution had a certain promotion effect on the cell viability of HFGs, and the highest cell viability of HFGs was observed when the concentration of PLA/TBC/Fe_3O_4 microsphere solution was 500 μg/mL. This demonstrates the excellent biocompatibility of PLA/TBC/Fe_3O_4 microspheres.

Fig. 6 displays H&E stained images of heart, liver, spleen, lung, and kidney sections from mice in the blank control group as well as mice consuming 1 mg/mL of PLA/TBC/Fe_3O_4 microspheres for 14 days. Compared with the blank control group, there was no significant difference in the organ sections of mice consuming 1 mg/mL of PLA/TBC/Fe_3O_4 microspheres, indicating that PLA/TBC/Fe_3O_4 microspheres have no obvious toxic side effects on mice and have good in vivo biocompatibility.

3.7. Evaluation of the effect of microspheres on dentin tubule closure

Having verified the magnetic orientation capability, shape memory function, and favorable biocompatibility of PLA/TBC/Fe_3O_4 microspheres, we proceeded to explore their potential for occluding dentinal tubules. To assess the sealing effect of PLA/TBC/Fe_3O_4 microspheres on dentinal tubules, as well as their penetration rate and closure rate within the tubules, we employed EDTA to remove the smear layer on the dentin surface after low-speed polishing, followed by ultrasonic cleaning. The treated dentin surface served as the blank control group for the dentinal tubule sealing experiment. Fig. 7(a) illustrates the utilization of the microspheres' shape memory functionality for dentinal tubule sealing. This process involves placing the microspheres in their temporary shape at the opening of the dentinal tubules and applying a directed magnetic field to facilitate the entry of ellipsoidal microspheres into the interior of the dentinal tubules. Once the microspheres reach a certain depth within the dentinal tubules, they are heated to revert back to their initial shape, completing the sealing process effectively.

Fig. S3 shows the teeth used in the experiment, and Longitudinal sections of teeth as well as the pictures of dentin sections. Fig. 7(b) (I) displays a cross-sectional SEM image of the dentinal tubules, exposing their orifices, while Fig. 7(b) (II) exhibits a longitudinal SEM image, revealing the hollow and open tubules arranged at intervals. Fig. 7(c) (I) illustrates the cross-sectional situation of microspheres stretched to 200 % of their own length entering the dentinal tubules under the influence of an external magnetic field, effectively sealing the majority of dentinal tubules through the open orifices. Fig. 7(c) (II) displays the longitudinal situation of microspheres stretched to 200 % of their length entering the dentinal tubules under the influence of an external magnetic field. The successful entry of microspheres into dentinal tubules, reaching a maximum depth of 29 μm, is evident from the observations. Considering the crucial role of tubule sealing in addressing dentin hypersensitivity, the microspheres in this experiment demonstrated an advantage in reaching deeper positions within the tubules under the influence of the magnetic field, thereby providing improved sealing capability.

Fig. 7(d) (I) and (II) present scanning electron microscope images showing the cross-sectional and longitudinal views of the experimental dentin discs after dentinal tubule occlusion and subsequent heating at

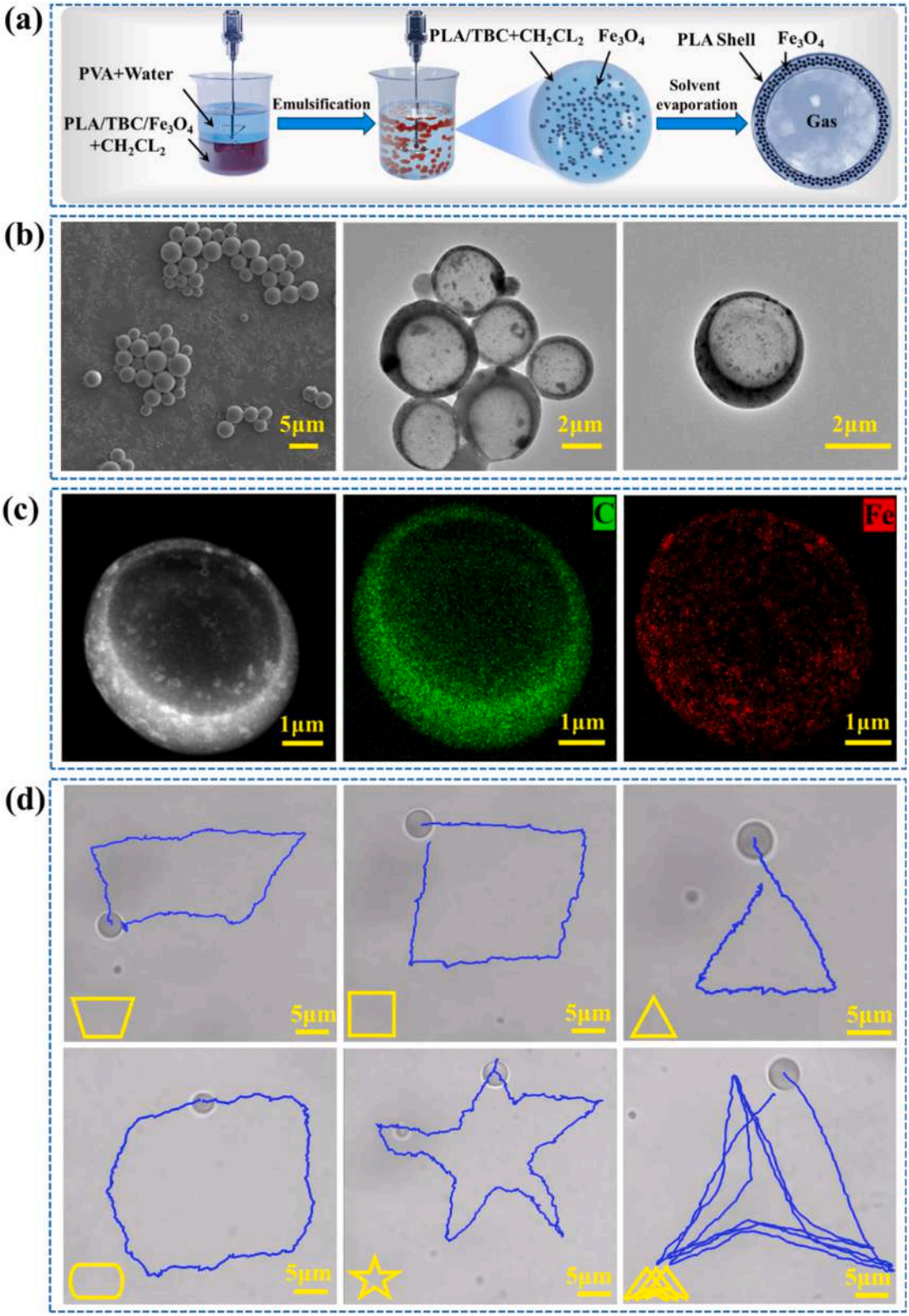

Fig. 4. (a) Preparation of PLA/TBC/Fe_3O_4 microspheres by emulsification-solvent evaporation method; (b) SEM and TEM images of PLA/TBC/Fe_3O_4 microspheres; (c) C and Fe elemental distribution of PLA/TBC/Fe_3O_4 microspheres; (d) The trajectory diagrams of PLA/TBC/Fe_3O_4 microspheres under the action of external magnetic field (the line in the figure is the trajectory diagram of microspheres under the action of magnetic field).

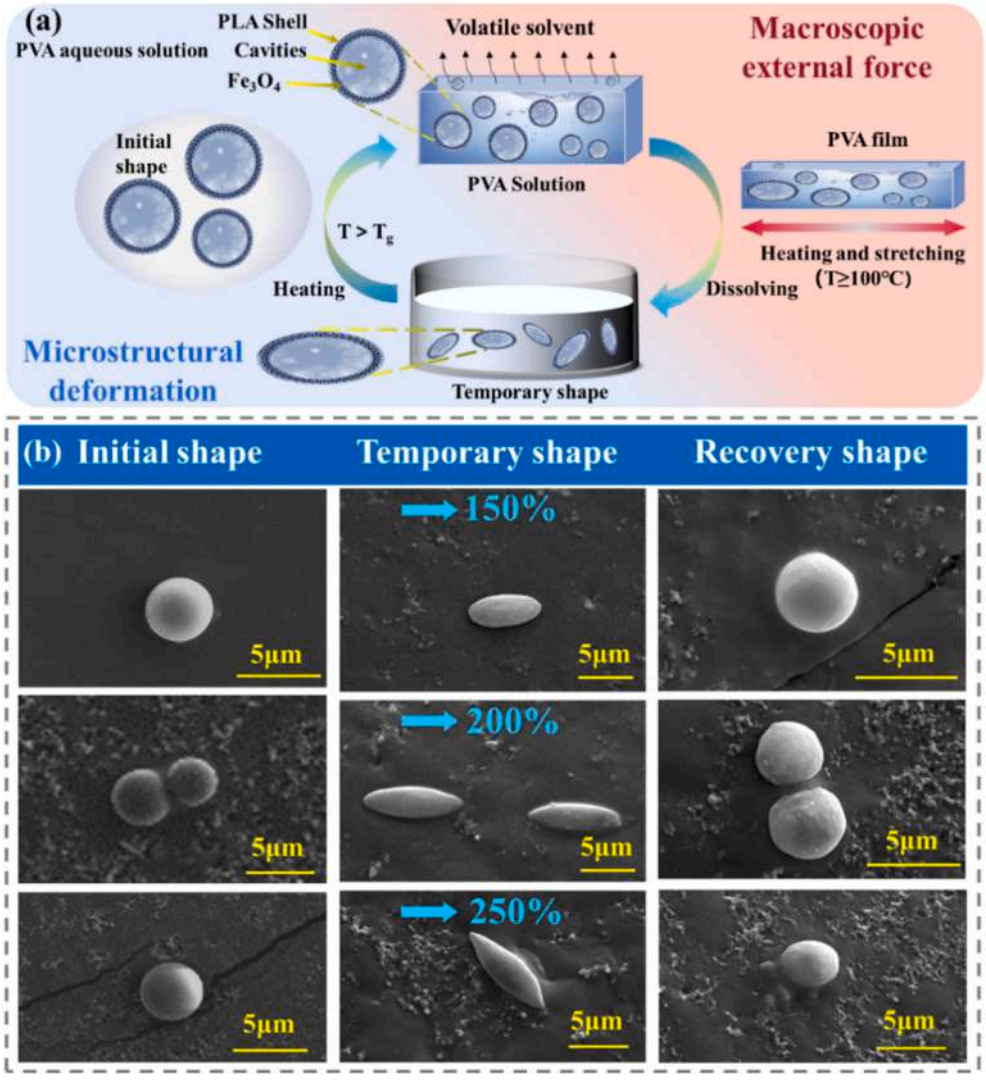

Fig. 5. (a) Schematic diagram of the shape memory process of PLA/TBC/Fe_3O_4 microspheres; (b) SEM image of shape memory of PLA/TBC/Fe_3O_4 microspheres (stretched ratio of 150–250%).

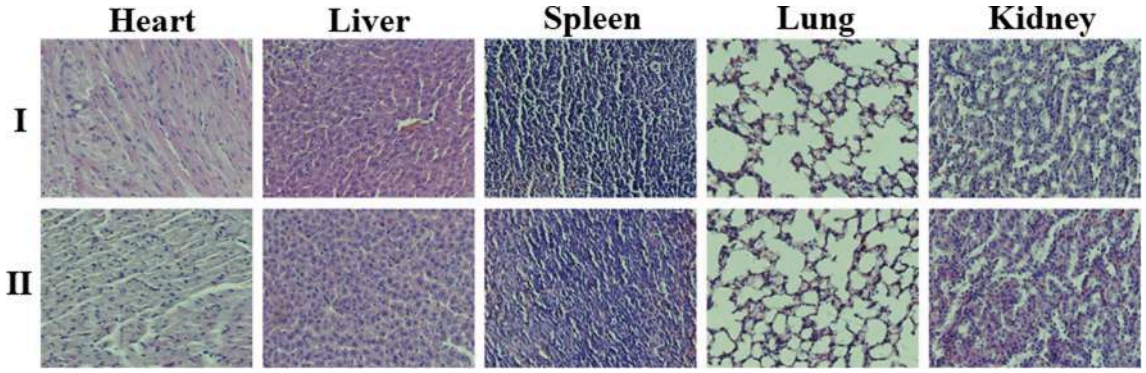

Fig. 6. Effects of PLA/TBC/Fe_3O_4 microspheres on the cells of various organs in mice (I is the blank control group, II is the experimental group fed with PLA/TBC/Fe_3O_4 microspheres).

40 °C for 60 s. Following heat treatment, microspheres that have been stretched to 200 % of their length return to their initial spherical shape. This observation indicates an enhanced sealing ability for the dentinal tubules, as evidenced by the increase in the short axis of the ellipsoidal microspheres, which returned to a spherical shape upon heating.

The comparison of dentinal tubule occlusion was conducted between microspheres under the influence of a magnetic field and those without it. Fig. S4 (I) represents the blank control group with no microspheres or magnetic fields. In Fig. S4 (II), microspheres sealed the dentinal tubules under the influence of an external magnetic field, effectively occluding the majority of dentinal tubules. However, in Fig. S4 (III), where microspheres attempted to seal dentinal tubules without a magnetic field,

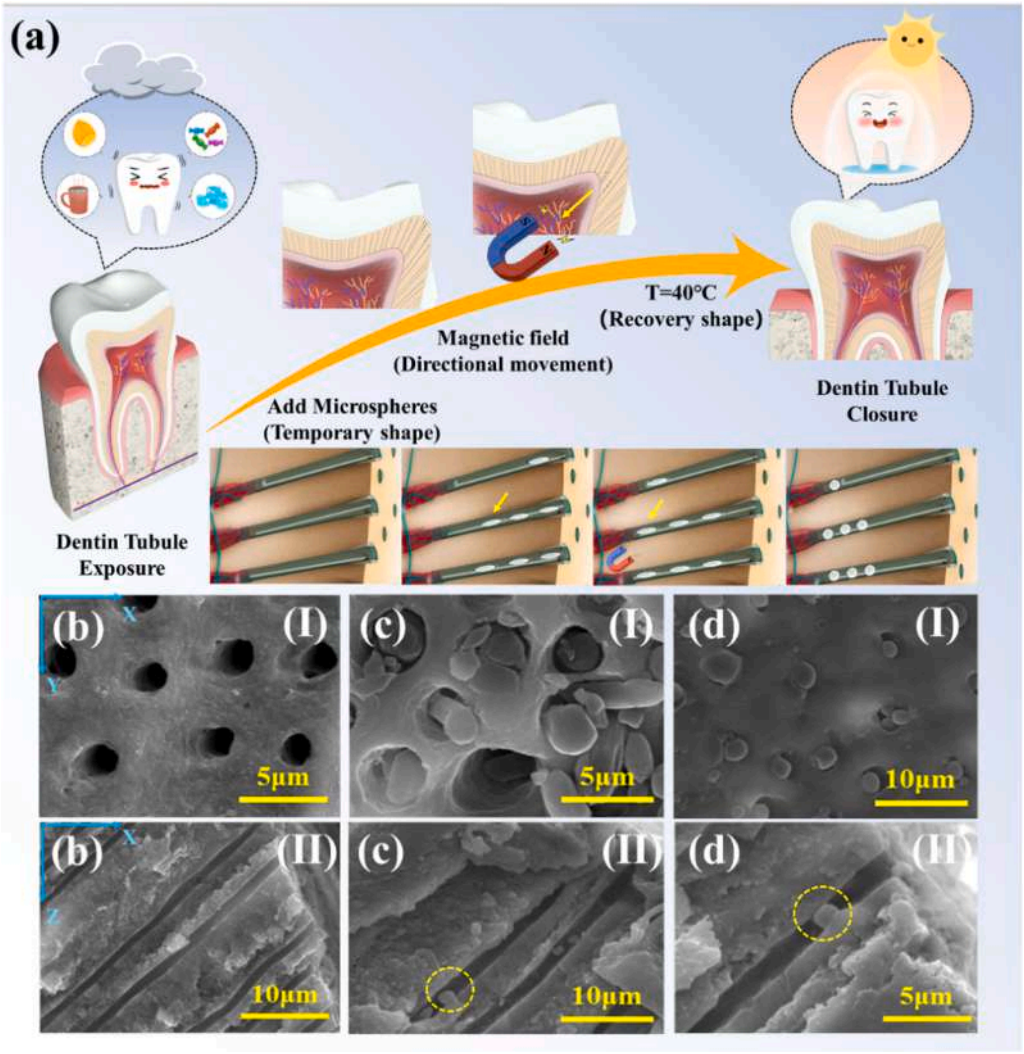

Fig. 7. (a) Diagram of the process of sealing dentin tubules by PLA/TBC/Fe_3O_4 microspheres; (b) (I) is an SEM image of a transverse section of a tooth slice (II) is an SEM image of a longitudinal section of a tooth slice; (c) (I) is an SEM image of a transverse section of an ellipsoidal microsphere after it enters a dentin tubule; (c) (II) SEM image of the longitudinal section of the ellipsoidal microspheres after entering the dentin tubules (d) (I) SEM image of the transverse section of the heated microspheres sealing the dentin tubules; (d) (II) SEM image of the longitudinal section of the heated microspheres sealing the dentin tubules.

most of the tubules remained open, with only a few containing microspheres. This finding indicates that microspheres exhibit significantly enhanced autonomous motion ability in the presence of a magnetic field, leading to a more effective occlusion of dentinal tubules.

Fig. S5 displays the statistical charts for the enrty rate (D_e) and sealing rate (D_s) of dentinal tubules with and without the influence of a magnetic field. In the absence of a magnetic field, microspheres demonstrated a sealing rate of 48.50 ± 7.69 % and entry rate of 70.56 ± 11.29 %. In contrast, when a magnetic field was present, microspheres exhibited notably higher sealing and entry rates of 85.41 ± 7.11 % and 93.33 ± 2.82 %, respectively. These findings provide evidence that microspheres displayed significantly improved penetration and closure capabilities when subjected to a magnetic field, thanks to their enhanced autonomous motion. This substantiates the considerable advantages of using magnetic field-assisted microspheres for dentinal tubule sealing, indicating promising prospects for addressing dentin hypersensitivity.

4. Conclusion

In this investigation, shape memory PLA/TBC/Fe_3O_4 microspheres were synthesized using PLA, TBC, and oleic acid-modified nano Fe_3O_4 particles as starting materials. The microspheres were produced through the O/W emulsion-solvent evaporation method, with their diameter tailored to match that of dentinal tubules. These microspheres exhibited autonomous movement when subjected to an applied magnetic field and demonstrated excellent shape recovery capabilities, reverting to their original shape at 40 °C. Cell viability and cytotoxicity experiments confirmed the biocompatibility of PLA/TBC/Fe_3O_4 microspheres and even showed that they promoted the proliferation of HGFs cells. Dentinal tubule sealing experiments demonstrated that the microspheres could effectively penetrate the dentinal tubules under the influence of the applied magnetic field, reaching a maximum depth of 29 μm. Once inside the tubules, the ellipsoidal shape memory PLA/TBC/Fe_3O_4 microspheres reverted to their initial shape, efficiently sealing the tubules. The magnetic field-assisted shape memory PLA/TBC/Fe_3O_4 microspheres exhibited a high entry rate of 93.33 ± 2.82 % and a sealing rate of 85.41 ± 7.11 % for dentinal tubule occlusion. These promising results suggest the potential application of the synthesized microspheres for effectively sealing dentinal tubules.

CRediT authorship contribution statement

Tao Guo: Data curation, Formal analysis, Investigation, Methodology, Writing – original draft. **Jiayuan Chen:** Formal analysis,

Investigation, Methodology. **Lan Luo:** Investigation, Methodology. **Qiangwang Geng:** Formal analysis, Methodology. **Linlin Wang:** Methodology. **Fenghua Zhang:** Conceptualization, Formal analysis, Investigation, Project administration, Supervision, Writing – review & editing. **Narisu Hu:** Investigation, Methodology, Project administration, Resources. **Yanju Liu:** Funding acquisition, Project administration. **Jinsong Leng:** Funding acquisition, Project administration, Supervision.

Declaration of competing interest

The authors declare that they have no known competing financial interests or personal relationships that could have appeared to influence the work reported in this paper.

Data availability

Data will be made available on request.

Acknowledgements

This work was supported by the National Natural Science Foundation of China (Grant No.12072094) and the National Key R&D Program of China (2022YFB3805700).

Appendix A. Supplementary material

Supplementary data to this article can be found online at https://doi.org/10.1016/j.compositesa.2024.108083.

References

[1] Liu Z, Li Q, Bian W, Lan X, Liu Y, Leng J. Preliminary Test and Analysis of An Ultralight Lenticular Tube Based on Shape Memory Polymer Composites. Compos Struct 2019;223:110936.
[2] Lin C, Lv J, Li Y, Zhang F, Li J, Liu Y, et al. 4D-printed Biodegradable and Remotely Controllable Shape Memory Occlusion Devices. Adv Funct Mater 2019;29(51):1906569.
[3] Zhang F, Wang L, Zheng Z, Liu Y, Leng J. Magnetic Programming of 4D-printed Shape Memory Composite Structures. Compos Part A-Appl Sci Manuf 2019;125:105571.
[4] Zhang Y, Zhang N, Hingorani H, Ding N, Wang D, Yuan C, et al. Fast-response, Stiffness-tunable Soft Actuator by Hybrid Multimaterial 3D Printing. Adv Funct Mater 2019;29(15):1806698.
[5] Yang H, D'Ambrosio N, Liu P, et al. Shape memory mechanical metamaterials. Mater Today 2023;66:36–49.
[6] Zhang C, Chen G, Zhang K, et al. Repeatedly Programmable Liquid Crystal Dielectric Elastomer with Multimodal Actuation. Adv Mater 2024:2313078.
[7] Peng W, Mu H, Liang X, et al. Digital Laser Direct Writing of Internal Stress in Shape Memory Polymer for Anticounterfeiting and 4D Printing. ACS Macro Lett 2023;12(12):1698–704.
[8] Wang J, Zhao Q, Wang Y, et al. Shape-Programmable Electronics: Self-Unfolding Flexible Microelectrode Arrays Based on Shape Memory Polymers. Adv Mater Technol 2019;4(11):1970063.
[9] Liu R, Dai H, Zhou Q, Zhang Q, Zhang P. Synthesis and Characterization of Shape-memory Poly Carbonate Urethane Microspheres for Future Vascular Embolization. J Biomater Sci-Polym Ed 2016;27(12):1248–61.
[10] Wischke C, Schossig M, Lendlein A. Shape-memory Effect of Micro-/nanoparticles from Thermoplastic Multiblock Copolymers. Small 2013;10(1):83–7.
[11] Wang L, Ma J, Guo T, Zhang F, Dong A, Zhang S, et al. Control of Surface Wrinkles on Shape Memory PLA/PPDO Micro-nanofibers and Their Applications in Drug Release and Anti-scarring. Adv Fiber Mater 2023;5(2):632–49.
[12] Nie M, Zhao Q, Du X. Recent advances in small-scale hydrogel-based robots for adaptive biomedical applications. Nano Res 2023:1–14.
[13] Li R, Wang Z, Li J, et al. Relieving thrombo-inflammation with acid-triggered polymersomes toward ischemic stroke therapy. Nano Today 2024;54:102114.
[14] Sun L, Zhou S, Wang W, et al. Preparation and characterization of porous biodegradable microspheres used for controlled protein delivery. Colloids Surf A Physicochem Eng Asp 2009;345(1–3):173–81.
[15] Zhao L, Xiao C, Wang L, Gai G, Ding J. Glucose-sensitive Polymer Nanoparticles for Self-regulated Drug Delivery. Chem Commun 2016;52(49):7633–52.
[16] Men J, Shi H, Dong C, Yang Y, Han Y, Wang R, et al. Preparation of Poly (Sodium 4-styrene Sulfonate) Grafted Magnetic Chitosan Microspheres for Adsorption of Cationic Dyes. Int J Biol Macromol 2021;181:810–23.
[17] Li G, He Y, Han W, Yu Y, Zhu L, Si T, et al. An Improved Solvent Evaporation Method to Produce Poly (Lactic Acid) Microspheres Via Foam-transfer. Int J Biol Macromol 2021;172:114–23.
[18] Mi F, Lin Y, Wu Y, Shyu S, Tsai Y. Chitin/PLGA Blend Microspheres as A Biodegradable Drug-delivery System: Phase-separation. Degradation Release Behav Biomater 2022;23(15):3257–67.
[19] Aydin O, Aydin B, Tezcaner A, Keskin D. Study on Physiochemical Structure and in Vitro Release Behaviors of Doxycycline-loaded PCL Microspheres. J Appl Polym Sci 2015;132(14):41768.
[20] Hou Y, Jiang N, Zhang L, Li Y, Meng Y, Han D, et al. Oppositely Charged Polyurethane Microspheres with Tunable Zeta Potentials as An Injectable Dual-loaded System for Bone Repair. ACS Appl Mater Interfaces 2017;9(31):25808–17.
[21] Roam J, Xu H, Nguyen P, Elbert D. The Formation of Protein Concentration Gradients Mediated by Density Differences of Poly (Ethylene Glycol) Microspheres. Biomaterials 2010;31(33):8642–50.
[22] Yuan X, Lin S, Zhao K, Han Y. Emulsion-ultrasonic Spray Method to Prepare Polylactic Acid Microspheres. Mater Lett 2022;309:131461.
[23] Xu J, Bai Y, Li X, Wei Z, Sun L, Yu H, et al. Porous Core/Dense Shell PLA Microspheres Embedded with High Drug Loading of Bupivacaine Crystals for Injectable Prolonged Release. AAPS PharmSciTech 2021;22:1–11.
[24] Zhan S, Zhang N, Zhao Q, Chen L, Chen S, Hou W. Preparation of The Magnetic Polylactic Acid Microspheres with The Modified Fe_3O_4 and Compound Emulsifiers. Particulate Sci Technol 2015;33(3):314–20.
[25] Zhong W, Zhang X, Duan X, Liu H, Fang Y, Luo M, et al. Redox-responsive self-assembled polymeric nanoprodrug for delivery of gemcitabine in B-cell lymphoma therapy. Acta Biomater 2022;144:67–80.
[26] McMillan A, Nguyen M, Huynh C, Sarett S, Ge P, Chetverikova M, et al. Hydrogel microspheres for spatiotemporally controlled delivery of RNA and silencing gene expression within scaffold-free tissue engineered constructs. Acta Biomater 2021;124:315–26.
[27] Zhou C, Ni Y, Liu W, Tan B, Yao M, Fang L, et al. Near-infrared light–induced sequential shape recovery and separation of assembled temperature memory polymer microparticles. Macromol Rapid Commun 2020;41(8):2000043.
[28] Li W, Liu Y, Leng J. Harnessing wrinkling patterns using shape memory polymer microparticles. Acs Appl Mater Interfaces 2020; 13(19): 23074–23080.
[29] Zhang F, Zhao T, Ruiz-Molina D, Liu Y, Roscini C, Leng J, et al. Shape Memory Polyurethane Microcapsules with Active Deformation. ACS Appl Mater Interfaces 2020;12(41):47059–64.
[30] Guo Q, Bishop C, Meyer R, Wilson D, Olasov L, Schlesinger D, et al. Entanglement-based Thermoplastic Shape Memory Polymeric Particles with Photothermal Actuation for Biomedical Applications. ACS Appl Mater Interfaces 2018;10(16):13333–41.
[31] Bai Y, Zhang J, Ju J, Liu J, Chen X. Shape Memory Microparticles with Permanent Shape Reconfiguration Ability and Near Infrared Light Responsiveness. Reactive Functional Polym 2020; 157: 104770.
[32] Li C, Zhang F, Zhao W, Wang L, Liu Y, Leng J. Preparation and Properties of Shape Memory PEG/IEM Resin and Its Composite Designed for Ureter Stent. Adv Healthcare Mater 2023; 12(16): 2300400.
[33] Lin C, Liu L, Liu Y, Leng J. Recent developments in next-generation occlusion devices. Acta Biomater 2021;128:100–19.
[34] Lin C, Huang Z, Wang Q, Zou Z, Wang W, Liu L, et al. 4D printing of overall radiopaque customized bionic occlusion devices. Adv Healthc Mater 2023;12(4):2201999.
[35] Simões T, Melo K, Fernandes-Neto J, Batista A, Silva M, Ferreira A, et al. Use of High-and Low-intensity Lasers in The Treatment of Dentin Hypersensitivity: A Literature Review. J Clin Exp Dentistry 2021;13(4):e412–7.
[36] Kumar N, Metha D. Short-term Assessment of The Nd: YAG Laser with and without Sodium Fluoride Varnish in The Treatment of Dentin Hypersensitivity-a Clinical and Scanning Electron Microscopy Study. J Periodontol 2005;76(7):1140–7.
[37] Bae J, Kim Y, Myung S. Desensitizing Toothpaste Versus Placebo for Dentin Hypersensitivity: A Systematic Review and Meta-analysis. J Clin Periodontol 2015;42(2):131–41.
[38] Rezazadeh F, Dehghanian P, Jafarpour D. Laser Effects on The Prevention and Treatment of Dentinal Hypersensitivity: A Systematic Review. J Lasers Med Sci 2019;10(1):1.
[39] Patil A, Varma S, Suragimath G, Abbayya K, Zope S, Kale V. Comparative Evaluation of Efficacy of Iontophoresis with 0.33% Sodium Fluoride Gel and Diode Laser Alone on Occlusion of Dentinal Tubules. J Clin Diagnostic Res: JCDR 2017;11(8): ZC123-ZC126.
[40] Rusin P, Agee K, Suchko M, Pashley D. Effect of A New Desensitizing Material on Human Dentin Permeability. Dent Mater 2010;26(6):600–7.